CHEMISTRY OF MATERIALS

Article

pubs.acs.org/cm

Increased Optoelectronic Quality and Uniformity of Hydrogenated p-InP Thin Films

Hsin-Ping Wang,[†,‡,§,∥,▽] Carolin M. Sutter-Fella,[†,‡,▽] Peter Lobaccaro,[#,+] Mark Hettick,[†,‡] Maxwell Zheng,[†,‡] Der-Hsien Lien,[†,‡,§,∥] D. Westley Miller,[⊥] Charles W. Warren,[⊥] Ellis T. Roe,[⊥] Mark C. Lonergan,[○] Harvey L. Guthrey,[¶] Nancy M. Haegel,[¶] Joel W. Ager,[‡] Carlo Carraro,[#] Roya Maboudian,[#] Jr-Hau He,[*,§] and Ali Javey[*,†,‡]

[†]Electrical Engineering and Computer Sciences and [#]Department of Chemical and Biomolecular Engineering, University of California, Berkeley, California 94720, United States

[‡]Materials Sciences Division and [+]Joint Center for Artificial Photosynthesis, Lawrence Berkeley National Laboratory, Berkeley, California 94720, United States

[§]Computer, Electrical and Mathematical Sciences and Engineering (CEMSE) Division, King Abdullah University of Science & Technology (KAUST), Thuwal 23955-6900, Saudi Arabia

[∥]Institute of Photonics and Optoelectronics & Department of Electrical Engineering, National Taiwan University, Taipei 10617, Taiwan

[⊥]Department of Physics and [○]Department of Chemistry and Biochemistry, University of Oregon, Eugene, Oregon 97403, United States

[¶]National Center for Photovoltaics (NCPV), National Renewable Energy Laboratory, Golden, Colorado 80401, United States

Supporting Information

ABSTRACT: The thin-film vapor−liquid−solid (TF-VLS) growth technique presents a promising route for high quality, scalable, and cost-effective InP thin films for optoelectronic devices. Toward this goal, careful optimization of material properties and device performance is of utmost interest. Here, we show that exposure of polycrystalline Zn-doped TF-VLS InP to a hydrogen plasma (in the following referred to as hydrogenation) results in improved optoelectronic quality as well as lateral optoelectronic uniformity. A combination of low temperature photoluminescence and transient photocurrent spectroscopy was used to analyze the energy position and relative density of defect states before and after hydrogenation. Notably, hydrogenation reduces the relative intragap defect density by 1 order of magnitude. As a metric to monitor lateral optoelectronic uniformity of polycrystalline TF-VLS InP, photoluminescence and electron beam induced current mapping reveal homogenization of the grain versus grain boundary upon hydrogenation. At the device level, we measured more than 260 TF-VLS InP solar cells before and after hydrogenation to verify the improved optoelectronic properties. Hydrogenation increased the average open-circuit voltage (V_{OC}) of individual TF-VLS InP solar cells by up to 130 mV and reduced the variance in V_{OC} for the analyzed devices.

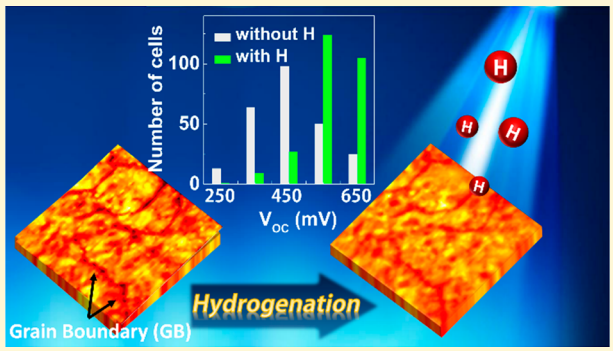

INTRODUCTION

InP is not only used in photocathodes,[1] photodetectors,[2] and lasers,[3,4] but it is also an attractive absorber material for thin-film solar cells due to its suitable optoelectronic properties, such as direct band gap, low unpassivated surface recombination velocity,[5] and high electron mobility. Its band gap of 1.34 eV ideally matches the terrestrial solar spectrum which translates into a theoretically maximum solar conversion efficiency of 31% (under terrestrial irradiation using a single p−n junction).[6] Our recently developed thin-film vapor−liquid−solid (TF-VLS) growth platform presents a promising route for the cost-effective fabrication of high quality InP.[7] In a first demonstration of device applications using the TF-VLS process, as grown InP was doped *p*-type with Zn by an ex-situ doping process and fabricated into solar cells. Promising efficiencies of up to 12.1% and a V_{OC} of 695 mV were obtained using a *n*-TiO_2/*p*-InP heterojunction architecture.[8] Despite these promising results, the V_{OC} is less than what has been reported for a InP wafer-based device, which displays a V_{OC} of 785 mV.[9]

Received: March 29, 2016
Revised: June 8, 2016

DOI: 10.1021/acs.chemmater.6b01257
Chem. Mater. XXXX, XXX, XXX−XXX

One obvious difference between a commercially available single crystal InP wafer and TF-VLS InP is the presence of grain boundaries. In general, grain boundaries can limit the optoelectronic properties of materials due to a high density of dangling bonds and impurity segregation caused by differences in diffusion behavior as compared to the bulk material.[10−12] Analyzing our TF-VLS *p*-InP via a combination of secondary ion mass spectroscopy (SIMS) and capacitance−voltage (CV) profiling revealed that only ∼10% of the incorporated Zn was electrically active in our TF-VLS *p*-InP, leading to the possibility that much of the interstitial Zn accumulates at the interfaces and along grain boundaries.[8] Moreover, the bulk material quality of single crystal InP can differ from thin-film InP as well, which is caused by structural differences inherent to the growth process such as dislocations, twin boundaries, and related defects.[13]

Hydrogen in semiconductors can play an important role by modifying the electrical properties of the material. It does so by passivating native defects and impurities or inducing electrically active defects. Furthermore, it shows amphoteric behavior in semiconductors, where H^+ acts as a donor in *p*-type and H^- as an acceptor in *n*-type semiconductors.[14,15] In III−V semiconductors, hydrogenation of GaAs improves the optoelectronic homogeneity and reduces the surface recombination velocity.[16] Exposure of single crystalline InP to a hydrogen plasma is an efficient method to passivate shallow acceptors and dislocations.[16−19] The latter, passivation of electrically active dislocations, leads to a reduction in trap states, and is accompanied by a narrowing of their energy distribution. The formation of neutral Zn−H complexes is proposed to explain the acceptor passivation.[17,20]

In this study, the effect of hydrogenation on the optoelectronic properties of Zn-doped TF-VLS InP (TF-VLS InP:Zn) was analyzed by low temperature photoluminescence (PL) measurements and transient photocurrent spectroscopy (TPI). In addition, the effect of hydrogenation on lateral optoelectronic uniformity was investigated using PL and electron beam-induced current (EBIC) mapping. Over all, hydrogenation induced defect passivation and enhanced optoelectronic uniformity translated into a V_{OC} increase accompanied by a narrowing of the V_{OC} distribution in TF-VLS InP solar cell devices.

EXPERIMENTAL SECTION

Figure 1 presents the process schematic of the hydrogenated TF-VLS InP. A 3 μm thick In film was evaporated on Mo foil and capped with a 40 nm SiO_2 layer to avoid dewetting of In from the Mo substrate during phosphorization at high temperature. The SiO_2 layer confines the film geometry while allowing P to diffuse into and react with the molten In film. InP growth was carried out at 700 °C for 20 min in a mixed phosphine/hydrogen gas (10% PH_3 diluted in 90% H_2) at a total pressure of 100 Torr. After the growth, the SiO_2 cap was etched away by HF. As-grown InP shows *n*-type behavior caused by donor-like P vacancies (V_P).[21,22]

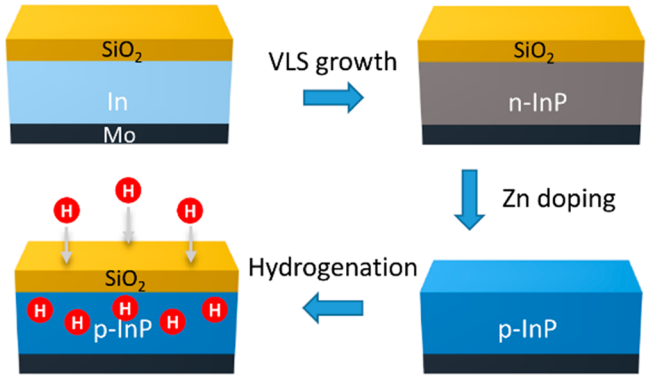

Figure 1. Schematic of the fabrication process of the TF-VLS InP with hydrogenation step after Zn doping.

The as-grown InP was converted to *p*-InP by vapor phase solid source doping using Zn_xP_y as the Zn source where the presence of gaseous P simultaneously suppresses surface decomposition. Within the InP lattice, Zn can substitute for In or occupy interstitial sites. Substitutional Zn atoms give rise to the observed *p*-type conductivity.[23] As outlined above, only ∼10% of the incorporated Zn is electrically active in our TF-VLS InP:Zn, i.e., Zn on In sites. Thus, a significant proportion of the Zn possibly forms precipitates or is incorporated as interstitial Zn. These Zn impurities can introduce deep recombination centers and thereby reduce the carrier diffusion length by increased recombination or by scattering-induced mobility loss.[24−26]

Following ex-situ doping of the InP, the samples were exposed to a H-plasma (Figure 1). Prior to hydrogenation, a 5 nm thick protective SiO_2 layer was deposited on InP to prevent surface damage and InP etching via the formation of PH_3 (Figure S1 in the Supporting Information). An inductively coupled plasma (ICP) was used as the plasma source for the hydrogen species. ICP plasma offers the benefit of being a gentle plasma source as compared to DC biased plasmas. Since there is no bias voltage applied, the treatment depends on the diffusivity of H species in InP. TF-VLS InP:Zn samples were exposed to an optimized condition of H-plasma at 15 W plasma power and 2 Torr chamber pressure for 5 min. The V_{OC} enhancement under different hydrogenation conditions is shown in Figure S2 in the Supporting Information. Following hydrogenation, the SiO_2 cap was etched away by HF. A *p-n* junction is required for some of the measurements presented below, thus, a 15 nm amorphous *n*-TiO_2 layer, acting as an electron selective contact, was deposited on the InP:Zn film by atomic layer deposition using titanium isopropoxide and water precursors at a temperature of 120 °C. Finally, a 55 nm ITO layer was sputtered on top of the *n*-TiO_2 as the transparent electrode, acting simultaneously as an antireflective layer to complete the stack (compare Figure 5a). EBIC analysis was done at an acceleration voltage of 30 kV and a beam current of ∼4 nA. Low temperature PL was done at 8 K with a 488 nm Ar ion laser excitation at 200 μW. PL mapping was performed with a 632.8 nm HeNe laser at 800 μW at room temperature. A Solar Light 16S 300W solar simulator was used as the light source at 1-sun intensity (100 mW/cm^2, AM1.5G) at room temperature to record the *J*−*V* curves. TPI spectroscopy, a form of subgap absorption spectroscopy, was used to characterize the energetic distribution of optically active defects in the band gap of TF-VLS InP photovoltaic devices.[27,28] In order to measure a TPI spectrum, a current transient was produced by holding the sample in reverse bias (−0.5 V) following a 100 ms filling pulse (+0.2 V). The samples were illuminated with monochromatic light during every other transient, and the TPI signal was calculated from the integrated difference between the illuminated and nonilluminated transients. By scanning the energy of the monochromatic illumination, and normalizing by the incident flux, a spectrum was produced.[29,30] Measurements were performed at 80 K.

RESULTS AND DISCUSSION

The optoelectronic properties of TF-VLS InP:Zn were investigated by low temperature PL. The PL spectra taken at 8 K on samples before and after hydrogenation, together with Gaussian fits of the data (dotted lines) are shown in Figure 2a. The fitted peaks are in agreement with previously reported PL spectra and can be attributed to various transitions based on those analyses. From high to low energy, they are band-to-acceptor (B-A) transition at 1.37 eV, the donor-to-acceptor (D-

DOI: 10.1021/acs.chemmater.6b01257
Chem. Mater. XXXX, XXX, XXX−XXX

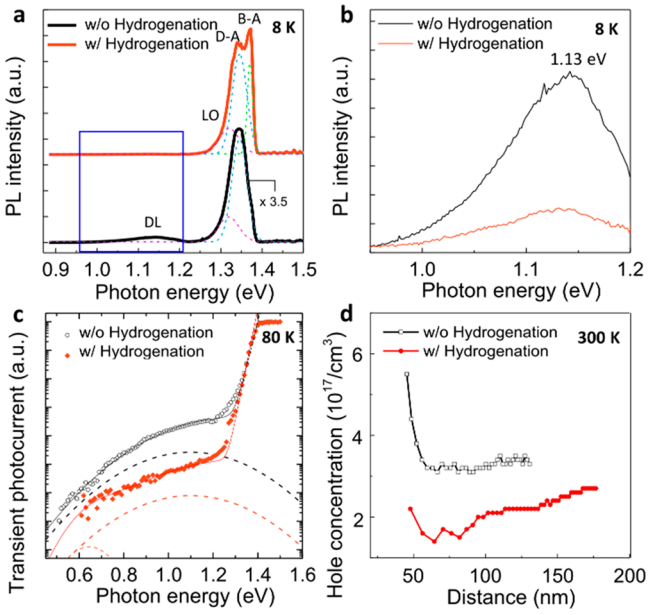

Figure 2. (a) PL spectra of TF-VLS InP:Zn (488 nm Ar ion laser excitation) at 8 K before and after hydrogenation. The fitted curves (dotted lines) are produced by using multiple-peak Gaussian fitting. (b) Enlargement of the broad DL peak seen in (a). (c) TPI spectra of TF-VLS InP solar cells with and without hydrogenation measured at 80 K under reverse bias of −0.5 V with filling pulse of 0.2 V. The solid lines represent fits with the integrated sum of two Gaussian defect bands and an exponential band edge. The dashed lines illustrate the underlying density of states. (d) Hole concentration as a function of depth extracted from CV measurements on completed devices before and after hydrogenation.

A) transition at 1.34 eV, a small longitudinal-optical phonon replica (LO) of the B-A transition at 1.32 eV, and a broad peak extending from 0.95 to 1.22 eV (centered around 1.13 eV) related to various deep levels (DLs).[31−34]

These DLs can be associated with V_P, interstitial Zn, residual impurities, and their complexes.[33,35] After hydrogenation, the absolute PL intensity associated with the DLs drops by a factor of 4 (Figure 2b), the B-A transition appears next to the D−A transition, and the near band edge transitions (D-A and B-A transitions) show a slight intensity increase. The reduction in DL intensity indicates that hydrogenation passivates DL related defect states within the band gap, while the appearance of the B-A transition and increased near band edge transition intensity imply reduced non-radiative recombination and, thus, increased radiative recombination.

The rollover of the exponential bandtail seen in the TPI spectra at high energies (Figure 2c) indicates a band gap of 1.41 eV at 80 K. An Urbach energy of 15 meV was extracted from the bandtail slope for both samples. This value compares favorably with Urbach energies reported for other polycrystalline thin-film solar cell materials. Values reported for CIGS range from 18 to 26 meV, for CdTe from 15 to 25 meV, and for CZTS from 13 to 31 meV.[27−30] At energies below the bandtail, the spectra of both samples are well fitted by the sum of two defect transitions occurring at 0.64 and 1.10 eV. For the sample without hydrogenation, the defect transition at 1.10 eV dominates the subgap absorption. The magnitude of the 1.10 eV defect response was reduced by a factor of ∼30 after hydrogenation. The energetic location of this transition and its reduced intensity after hydrogenation are in good agreement with the diminished DL response seen in the low temperature PL spectra.

Following the defect study, the effect of hydrogenation on the net hole concentration in InP:Zn was analyzed by CV measurements. To reduce the series resistance, a 100 nm Au layer was deposited on top of the completed devices (Au/ITO/n-TiO_2/p-InP/Mo). A 1 × 1 mm^2 active cell area was defined by patterning the front contact using lithography. Figure 2d illustrates the hole concentration in TF-VLS InP:Zn before and after hydrogenation. After hydrogenation, there is a slight decrease in hole concentration, from ∼3.5 × 10^{17} cm^{-3} in the untreated sample to ∼2 × 10^{17} cm^{-3} in the hydrogenated sample. This slight reduction in hole concentration after hydrogenation was observed consistently in more than 10 samples, indicating a statistical difference. Moreover, the hole concentration at the surface is about three times lower after hydrogenation. Zn accumulation at the InP surface might limit the electron transport from InP to TiO_2 due to an unfavorable band bending, which could lead to high charge carrier recombination, resulting in a V_{OC} loss.[8,23] The beneficial reduction in hole concentration after hydrogenation could be explained by a neutralization reaction where substitutional Zn (Zn^- acceptor) forms an electrically neutral complex with hydrogen: $H^+ + Zn^- \rightarrow (ZnH)^0$.[17,36]

Next, the influence of hydrogenation on charge carrier collection in the completed solar cell devices was investigated by EBIC top-view mapping. In the EBIC technique, the electron−hole pairs are generated by scanning the electron beam across the sample and are separated by the built-in electric field.[37] Figure 3a−c presents a top-view SEM image and

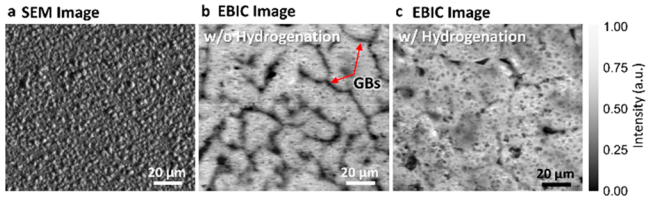

Figure 3. (a) SEM top view image of a TF-VLS InP solar cell. (b, c) Top view EBIC images of TF-VLS InP solar cells without and with hydrogenation. The charge carrier collection is visualized by the EBIC maps. Bright areas indicate higher collection efficiency of minority carriers. Grain boundaries are visible as dark lines.

the EBIC maps of TF-VLS InP devices with and without hydrogenation, respectively. The image intensity represents the local collection efficiency of charge carriers generated by the sample under scanning electron beam excitation at each pixel. Bright areas in the EBIC images indicate higher collection efficiency of minority carriers. The dark lines in the image of the sample before hydrogenation (Figure 3b) depict poor carrier collection along grain boundaries likely due to a higher concentration of non-radiative recombination centers.[38] Figure 3c shows that hydrogenation helps to improve charge carrier collection over grain boundaries. One possible explanation for this is that most of the electrically active Zn or other impurities that segregate along grain boundaries[39] are neutralized by the hydrogenation, thus improving carrier transport and collection. The neutralization mechanism could be interpreted by hydrogen bonding to electrically active Zn or impurities, via the formation of electrically inactive neutral complexes, which passivate the active grain boundaries.[17,36]

DOI: 10.1021/acs.chemmater.6b01257
Chem. Mater. XXXX, XXX, XXX−XXX

We then studied the optical uniformity of the material via PL mapping. Figure 4 shows normalized PL maps of the TF-VLS

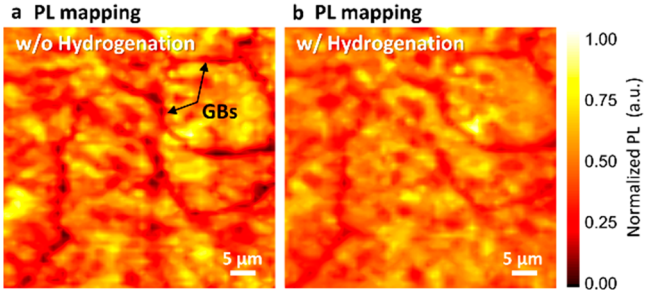

Figure 4. Room-temperature PL mapping of TF-VLS InP:Zn on the same area (HeNe laser excitation source at 632.8 nm) (a) before and (b) after hydrogenation. The PL intensities are normalized to the maximum intensity of each PL map, and the standard deviation before and after hydrogenation are 130 and 63 counts, respectively.

InP:Zn before and after hydrogenation recorded at the same location on the film. After hydrogenation, the initially dark grain boundaries show a relative increase in PL signal. Consequently, the PL signal becomes more uniform over the mapped area, resulting in a reduced standard deviation. In combination with the EBIC analysis, this result leads to the conclusion that hydrogenation helps to form optoelectronically more benign grain boundaries.

The influence of hydrogenation at the device level is depicted in Figure 5. Figure 5a illustrates a schematic of the device stack and Figure 5b depicts the dark and illuminated current density versus voltage ($J-V$) measurements. From the $J-V$ curves of an

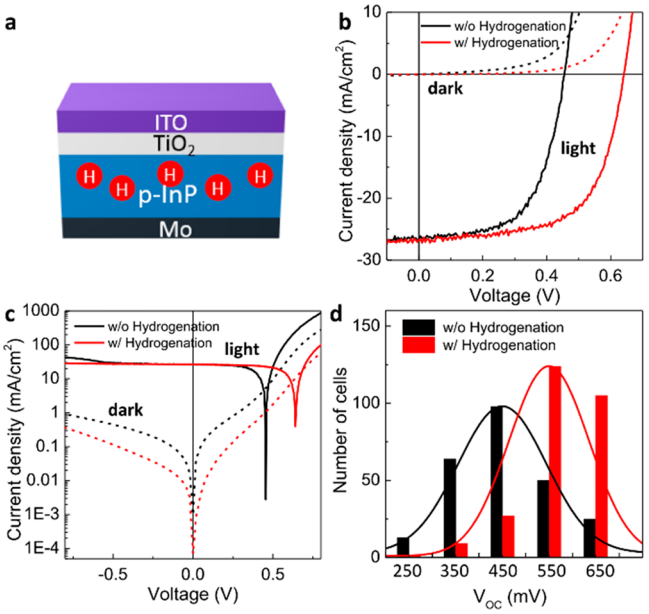

Figure 5. (a) Schematic of the InP solar cell device stack (ITO/*n*-TiO_2/*p*-InP/Mo). (b) $J-V$ characteristic for TF-VLS InP solar cells with and without hydrogenation under simulated 1 sun illumination (solid line) and in the dark (dash line) at room temperature. Cell area was 0.5 × 0.5 mm^2. (c) Logarithmic plot of (b). The reverse currents are plotted as positive values. (d) Histogram of the V_{OC} distribution of TF-VLS InP solar cells with and without hydrogenation. The V_{OC}'s are binned into 100 mV intervals. The fitted curves are produced by Gaussian fitting.

average device under illumination, one can see that the V_{OC} shows pronounced improvements from 455 to 635 mV after hydrogenation. One reason for the clear V_{OC} increase is the significant suppression of dark current after hydrogenation (Figure 5c) which is almost up to 1 order of magnitude lower compared to the untreated sample. Moreover, the shunt resistance of 456 Ω cm^2 increases to 2837 Ω cm^2, which is extracted by fitting the slope past short circuit from the dark current. In a polycrystalline material, the shunting behavior could be caused by two main reasons: the presence of grain boundaries or highly localized shunt regions.[40] Grain boundaries are a likely origin of shunt paths.[41] If the grain boundaries are type inverted, they directly connect the *n*-type TiO_2 to the metallic back contact, causing a leakage current. After hydrogenation of TF-VLS InP, the shunt resistance and V_{OC} increase dramatically, indicating the electronic activity of grain boundaries and localized defects is passivated by hydrogen, suppressing extensive dark current flow.

Further analysis of the $J-V$ measurements reveals almost the same short-circuit current density (26.6 and 26.7 mA/cm^2) but improved fill factor from 59% to 64% related to the significant V_{OC} and shunt resistance increase. This results in a conversion efficiency of 10.8% for the hydrogenated device, a marked improvement from 7.1% before hydrogenation.

Figure 5d illustrates the V_{OC} distribution of 267 TF-VLS InP solar cells with their Gaussian fits (that serve as a guide for the eye) before and after hydrogenation to verify the improved optoelectronic properties. More precisely, a histogram is shown with the experimental V_{OC} values binned by a 100 mV window. With hydrogenation, the average V_{OC} is 570 mV compared to an average of 441 mV without hydrogenation. The corresponding standard deviation dropped to 83 mV compared to a standard deviation of 118 mV without hydrogenation. Although the conversion efficiency does not overcome the reported record device performance,[8] this finding reinforces the idea that hydrogen passivation significantly enhances optoelectronic uniformity accompanied by a narrowing of the V_{OC} distribution in TF-VLS InP solar cell devices.

CONCLUSION

In conclusion, we have demonstrated that hydrogenation is an effective method to increase the optoelectronic quality and the lateral optoelectronic uniformity of TF-VLS InP:Zn. Low temperature PL measurements in combination with transient photocurrent spectroscopy showed the reduction of sub-band gap states. Electrical CV measurements revealed a decrease in net bulk and surface hole concentration after hydrogenation, thus supporting the formation of electrically neutral Zn−H complexes $(ZnH)^0$. Additionally, PL and EBIC mapping provided evidence for more uniform charge carrier collection after hydrogenation, suggesting that hydrogenation results in grain boundaries that are more electrically benign. The higher optoelectronic quality and uniformity directly translate to an average V_{OC} enhancement of more than 100 mV as well as a reduction in V_{OC} variation from sample-to-sample. This result outlines a promising method for the improvement of nonepitaxial III−V thin-films for future optoelectronic applications.

DOI: 10.1021/acs.chemmater.6b01257
Chem. Mater. XXXX, XXX, XXX−XXX

■ ASSOCIATED CONTENT

Supporting Information

The Supporting Information is available free of charge on the ACS Publications website at DOI: 10.1021/acs.chemmater.6b01257.

$J-V$ of InP with and without SiO_2 cap protection, degradation of the surface due to reaction of phosphorus with hydrogen and the subsequent formation of PH_3. Effect of hydrogen concentration. V_{OC} enhancement under different hydrogenation conditions, including different power and exposure times (PDF)

■ AUTHOR INFORMATION

Corresponding Authors

*(J.-H.H.) E-mail: jrhau.he@kaust.edu.sa.
*(A.J.) E-mail: ajavey@eecs.berkeley.edu.

Author Contributions

All authors have given approval to the final version of the manuscript.

Author Contributions

∇(H.-P.W. and C.M.S.-F.) These authors contributed equally.

Notes

The authors declare no competing financial interest.

■ ACKNOWLEDGMENTS

Materials characterization and growth was supported by the Electronic Materials Program funded by the Office of Science, Office of Basic Energy Sciences, of the U.S. Department of Energy, under Contract No. DE-AC02-05CH11231. Device fabrication was supported by the Department of Energy through the Bay Area Photovoltaic Consortium under Award Number DE-EE0004946. J.-H.H. acknowledges KAUST and National Science Council of Taiwan (NSC 102-2911-I-002-552). C.M.S.-F. acknowledges financial support from the Swiss National Science Foundation (P2EZP2_155586).

■ REFERENCES

(1) Hettick, M.; Zheng, M.; Lin, Y.; Sutter-Fella, C. M.; Ager, J. W.; Javey, A. Nonepitaxial Thin-Film InP for Scalable and Efficient Photocathodes. *J. Phys. Chem. Lett.* **2015**, *6*, 2177−2182.

(2) Beling, A.; Campbell, J. C. InP-Based High-Speed Photodetectors. *J. Lightwave Technol.* **2009**, *27*, 343−355.

(3) Li, K.; Sun, H.; Ren, F.; Ng, K. W.; Tran, T. T. D.; Chen, R.; Chang-Hasnain, C. J. Tailoring the Optical Characteristics of Microsized InP Nanoneedles Directly Grown on Silicon. *Nano Lett.* **2014**, *14*, 183−190.

(4) Soda, H.; Iga, K.-i.; Kitahara, C.; Suematsu, Y. GaInAsP/InP Surface Emitting Injection Lasers. *Jpn. J. Appl. Phys.* **1979**, *18*, 2329−2330.

(5) Wallentin, J.; Anttu, N.; Asoli, D.; Huffman, M.; Åberg, I.; Magnusson, M. H.; Siefer, G.; Fuss-Kailuweit, P.; Dimroth, F.; Witzigmann, B.; Xu, H. Q.; Samuelson, L.; Deppert, K.; Borgström, M. T. InP Nanowire Array Solar Cells Achieving 13.8% Efficiency by Exceeding the Ray Optics Limit. *Science* **2013**, *339*, 1057−1060.

(6) Henry, C. H. Limiting Efficiencies of Ideal Single and Multiple Energy Gap Terrestrial Solar Cells. *J. Appl. Phys.* **1980**, *51*, 4494−4500.

(7) Kapadia, R.; Yu, Z.; Wang, H.-H. H.; Zheng, M.; Battaglia, C.; Hettick, M.; Kiriya, D.; Takei, K.; Lobaccaro, P.; Beeman, J. W.; Ager, J. W.; Maboudian, R.; Chrzan, D. C.; Javey, A. A Direct Thin-Film Path Towards Low-Cost Large-Area III-V Photovoltaics. *Sci. Rep.* **2013**, *3*, 2275.

(8) Zheng, M.; Wang, H. P.; Sutter-Fella, C. M.; Battaglia, C.; Aloni, S.; Wang, X.; Moore, J.; Beeman, J. W.; Hettick, M.; Amani, M.; Hsu, W. T.; Ager, J. W.; Bermel, P.; Lundstrom, M.; He, J. H.; Javey, A. Thin-Film Solar Cells with InP Absorber Layers Directly Grown on Nonepitaxial Metal Substrates. *Adv. Energy Mater.* **2015**, *5*, 1501337.

(9) Yin, X.; Battaglia, C.; Lin, Y.; Chen, K.; Hettick, M.; Zheng, M.; Chen, C. Y.; Kiriya, D.; Javey, A. 19.2% Efficient InP Heterojunction Solar Cell with Electron-Selective TiO_2 Contact. *ACS Photonics* **2014**, *1*, 1245−1250.

(10) Thompson, K.; Booske, J. H.; Larson, D. J.; Kelly, T. F. Three-Dimensional Atom Mapping of Dopants in Si Nanostructures. *Appl. Phys. Lett.* **2005**, *87*, 052108.

(11) Thompson, K.; Bunton, J. H.; Kelly, T. F.; Larson, D. J. Characterization of Ultralow-Energy Implants and Towards the Analysis of Three-Dimensional Dopant Distributions Using Three-Dimensional Atom-Probe Tomography. *J. Vac. Sci. Technol. B* **2006**, *24*, 421−427.

(12) Johnson, N. M.; Biegelsen, D. K.; Moyer, M. D. Deuterium Passivation of Grain-Boundary Dangling Bonds in Silicon Thin Films. *Appl. Phys. Lett.* **1982**, *40*, 882−884.

(13) Friedrich, J.; Kallinger, B.; Knoke, I.; Berwian, P.; Meissner, E. Crystal Growth of Compound Semiconductors with Low Dislocation Densities. *20th Indium Phosphide and Related Materials (IPRM)* **2008**, 1−6.

(14) Van de Walle, C. G.; Neugebauer, J. Hydrogen in Semiconductors. *Annu. Rev. Mater. Res.* **2006**, *36*, 179−198.

(15) Van de Walle, C. G.; Neugebauer, J. Universal Alignment of Hydrogen Levels in Semiconductors, Insulators and Solutions. *Nature* **2003**, *423*, 626−628.

(16) Omeljanovsky, E. M.; Pakhomov, A. V.; Polyakov, A. Y. Hydrogen Passivation of Defects and Impurities in GaAs and InP. *J. Electron. Mater.* **1989**, *18*, 659−670.

(17) Chevallier, J.; Jalil, A.; Theys, B.; Pesant, J. C.; Aucouturier, M.; Rose, B.; Mircea, A. Hydrogen Passivation of Shallow Acceptors in *p*-Type InP. *Semicond. Sci. Technol.* **1989**, *4*, 87−90.

(18) Dautremont-Smith, W. C.; Lopata, J.; Pearton, S. J.; Koszi, L. A.; Stavola, M.; Swaminathan, V. Hydrogen Passivation of Acceptors in p-InP. *J. Appl. Phys.* **1989**, *66*, 1993−1996.

(19) Chatterjee, B.; Ringel, S. A.; Sieg, R.; Hoffman, R.; Weinberg, I. Hydrogen Passivation of Dislocations in InP on GaAs Heterostructures. *Appl. Phys. Lett.* **1994**, *65*, 58−60.

(20) McMurray, R. E., Jr; Haegel, N. M.; Kahn, J. M.; Haller, E. E. Beryllium-Hydrogen and Zinc-Hydrogen Shallow Acceptor Complexes in Germanium. *Solid State Commun.* **1987**, *61*, 27−32.

(21) Tsai, M. J.; Fahrenbruch, A. L.; Bube, R. H. Sputtered Oxide/Indium Phosphide Junctions and Indium Phosphide Surfaces. *J. Appl. Phys.* **1980**, *51*, 2696−2705.

(22) Temkin, H.; Dutt, B. V.; Bonner, W. A.; Keramidas, V. G. Deep Radiative Levels in InP. *J. Appl. Phys.* **1982**, *53*, 7526−7533.

(23) Tuck, B.; Hooper, A. Diffusion Profiles of Zinc in Indium Phosphide. *J. Phys. D: Appl. Phys.* **1975**, *8*, 1806−1821.

(24) van Gurp, G. J.; van Dongen, T.; Fontijn, G. M.; Jacobs, J. M.; Tjaden, D. L. A. Interstitial and substitutional Zn in InP and InGaAsP. *J. Appl. Phys.* **1989**, *65*, 553−560.

(25) Asakawa, K. Indium Phosphide and Related Materials: Processing, Technology, and Devices. *Adv. Mater.* **1993**, *5*, 228−229.

(26) Grabmaier, J. G. *Silicon*; Springer-Verlag Berlin and Heidelberg GmbH: Berlin, Germany, 2013.

(27) Warren, C. W.; Li, J.; Wolden, C. A.; Meysing, D. M.; Barnes, T. M.; Miller, D. W.; Heath, J. T.; Lonergan, M. C. The Effect of Copper on the Sub-Bandgap Density of States of CdTe Solar Cells. *Appl. Phys. Lett.* **2015**, *106*, 203903.

(28) Miller, D. W.; Warren, C. W.; Gunawan, O.; Gokmen, T.; Mitzi, D. B.; Cohen, J. D. Electronically Active Defects in the $Cu_2ZnSn(Se,S)_4$ Alloys as Revealed by Transient Photocapacitance Spectroscopy. *Appl. Phys. Lett.* **2012**, *101*, 142106.

(29) Boucher, J. W.; Miller, D. W.; Warren, C. W.; Cohen, J. D.; McCandless, B. E.; Heath, J. T.; Lonergan, M. C.; Boettcher, S. W. Optical Response of Deep Defects as Revealed by Transient Photocapacitance and Photocurrent Spectroscopy in CdTe/CdS Solar Cells. *Sol. Energy Mater. Sol. Cells* **2014**, *129*, 57−63.

DOI: 10.1021/acs.chemmater.6b01257
Chem. Mater. XXXX, XXX, XXX−XXX

(30) Heath, J. T.; Cohen, J. D.; Shafarman, W. N.; Liao, D. X.; Rockett, A. A. Effect of Ga Content on Defect States in $CuIn_{1-x}Ga_xSe_2$ Photovoltaic Devices. *Appl. Phys. Lett.* **2002**, *80*, 4540−4542.
(31) Montie, E. A.; van Gurp, G. J. Photoluminescence of Zn-diffused and Annealed InP. *J. Appl. Phys.* **1989**, *66*, 5549−5553.
(32) Hsu, J. K.; Juang, C.; Lee, B. J.; Chi, G. C. Photoluminescence Studies of Interstitial Zn in InP due to Rapid Thermal Annealing. *J. Vac. Sci. Technol., B: Microelectron. Process. Phenom.* **1994**, *12*, 1416−1418.
(33) Banerjee, S.; Srivastava, A. K.; Arora, B. M. Thermal Degradation of InP in Open Tube Processing: Deep-Level Photoluminescence. *J. Appl. Phys.* **1990**, *68*, 2324−2330.
(34) Swaminathan, V.; Donnelly, V. M.; Long, J. A Photoluminescence Study of Cd-Related Centers in InP. *J. Appl. Phys.* **1985**, *58*, 4565−4572.
(35) Mullin, J. B.; Royle, A.; Straughan, B. W.; Tufton, P. J.; Williams, E. W. Crystal Growth and Properties of Group IV Doped Indium Phosphide. *J. Cryst. Growth* **1972**, *13*, 640−646.
(36) Pearton, S. J.; Corbett, J. W.; Shi, T. S. Hydrogen in Crystalline Semiconductors. *Appl. Phys. A: Solids Surf.* **1987**, *43*, 153−195.
(37) Holt, D. B.; Joy, D. C. *SEM Microcharacterization of Semiconductors*; Academic: 1986.
(38) Chen, J.; Sekiguchi, T.; Yang, D.; Yin, F.; Kido, K.; Tsurekawa, S. Electron-Beam-Induced Current Study of Grain Boundaries in Multicrystalline Silicon. *J. Appl. Phys.* **2004**, *96*, 5490−5495.
(39) Heitjans, P.; Kȓger, J. *Diffusion in Condensed Matter: Methods, Materials, Models*; Springer: Berlin, Germany, 2005.
(40) Virtuani, A.; Lotter, E.; Powalla, M.; Rau, U.; Werner, J. H.; Acciarri, M. Influence of Cu Content on Electronic Transport and Shunting Behavior of $Cu(In,Ga)Se_2$ Solar Cells. *J. Appl. Phys.* **2006**, *99*, 014906.
(41) Thibault, J.; Rouviere, J.-L.; Bourret, A. *Grain Boundaries in Semiconductors*, In *Handbook of Semiconductor Technology*; Wiley-VCH Verlag GmbH: 2008; pp 377−451.

DOI: 10.1021/acs.chemmater.6b01257
Chem. Mater. XXXX, XXX, XXX−XXX

Supporting Information

Increased Optoelectronic Quality and Uniformity of Hydrogenated p-InP Thin Films

Hsin-Ping Wang,[†,‡,§,∥,∇] Carolin M. Sutter-Fella,[†,‡,∇] Peter Lobaccaro,[#,+] Mark Hettick,[†,‡,] Maxwell Zheng,[†,‡] Der-Hsien Lien,[†,‡,§,∥] D. Westley Miller,[⊥] Charles W. Warren,[⊥] Ellis T. Roe,[⊥] Mark C. Lonergan,[¥] Harvey L. Guthrey,[Δ] Nancy M. Haegel,[Δ] Joel W. Ager,[‡] Carlo Carraro,[#] Roya Maboudian,[#] Jr-Hau He[*,§] and Ali Javey[*,†,‡]

[†] Electrical Engineering and Computer Sciences, University of California, Berkeley, California 94720, United States

[‡] Materials Sciences Division, Lawrence Berkeley National Laboratory, Berkeley, California 94720, United States

[#] Department of Chemical and Biomolecular Engineering, University of California, Berkeley, California 94720, United States

[+] Joint Center for Artificial Photosynthesis, Lawrence Berkeley National Laboratory, Berkeley, California 94720, United States

[§] Computer, Electrical and Mathematical Sciences and Engineering (CEMSE) Division, King Abdullah University of Science & Technology (KAUST), Thuwal 23955-6900, Saudi Arabia

[∥] Institute of Photonics and Optoelectronics & Department of Electrical Engineering, National Taiwan University, Taipei 10617, Taiwan

[⊥] Department of Physics, University of Oregon, Eugene, Oregon 97403, United States

[¥] Department of Chemistry and Biochemistry, University of Oregon, Eugene, Oregon 97403, United States

[Δ] National Center for Photovoltaics (NCPV), National Renewable Energy Laboratory, Golden, Colorado 80401, United States

Effect of SiO_2 cap protection during hydrogenation. Prior to hydrogenation, a protective SiO_2 layer was deposited on InP to prevent surface damage and InP etching via the formation of PH_3. Figure S1 shows the *J-V* characteristic for TF-VLS InP solar cells with different cap thicknesses. InP capped with 2 and 5 nm SiO_2 results in the same *J-V* characteristic. However, exposure of InP to a hydrogen plasma without cap protection leads to a rapid degradation of the surface due to the reaction of phosphorus with hydrogen and the subsequent formation of PH_3, resulting in P deficient surface and a strong degradation of device performance.

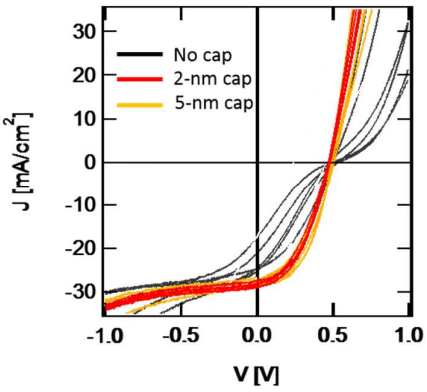

Figure S1 *J-V* characteristic for TF-VLS InP solar cells with different cap thickness (plasma condition: 15 W at 2 Torr, 5 minutes).

Effect of hydrogen concentration. The hydrogen concentration in *p*-InP does affect the impact of passivation. The plasma density can be controlled by power and gas pressure. Figure S2 shows the V_{OC} enhancement with different power and exposure times. The V_{OC} of InP solar cells increases for increasing plasma power from 5 to 15 W before it drops again at 20 W at constant exposure for 10 minutes. With increasing plasma power, the H concentration is expected to be higher and at the same time the diffusion depth is larger. Thus, there might be two effects coming into play: passivation of Zn at the TiO_2/InP interface as well as at the InP/Mo interface. Zn at the back interface is probably facilitating hole transport but might be passivated at high plasma power leading to a *Voc* reduction.

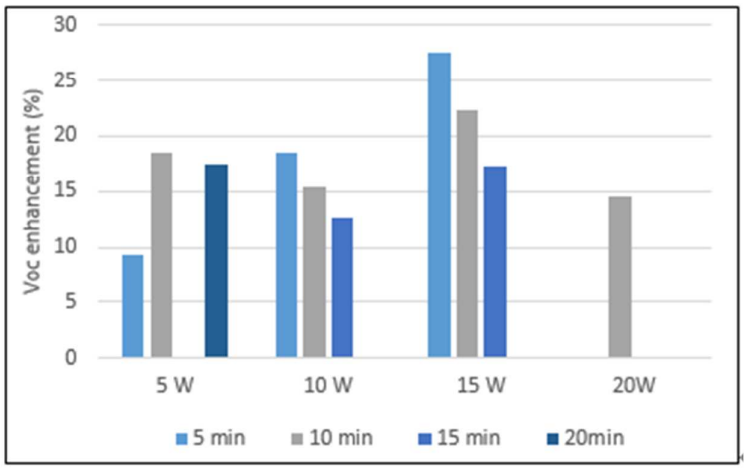

Figure S2 The V_{OC} enhancement with different plasma power and exposure time.